Effects of spin-orbit coupling on quantum transport

Bardarson, J.H.

Chapter 6

One-Parameter Scaling at the Dirac Point in Graphene

6.1 Introduction

Graphene provides a new regime for two-dimensional quantum transport [23–25], governed by the absence of backscattering of Dirac fermions [22]. A counterintuitive consequence is that adding disorder to a sheet of undoped graphene initially *increases* its conductivity [38, 109]. Intervalley scattering at stronger disorder strengths enables backscattering [110], eventually leading to localization and to a vanishing conductivity in the thermodynamic limit [36, 37]. Intervalley scattering becomes less and less important if the disorder is more and more smooth on the scale of the lattice constant a. The fundamental question of the new quantum transport regime is how the conductivity σ scales with increasing system size L if intervalley scattering is suppressed.

In usual disordered electronic systems, the hypothesis of *one-parameter scaling* plays a central role in our conceptual understanding of the metal-insulator transition [34, 111]. According to this hypothesis, the logarithmic derivative $d\ln\sigma/d\ln L = \beta(\sigma)$ is a function only of σ itself[1] — irrespective

[1] We define the β-function in terms of the ensemble averaged conductivity σ, measured in units of $4e^2/h$ (with the factor of four accounting for twofold spin and valley degeneracies). This is the appropriate definition for our system. For a more general definition of one-parameter scaling, one needs to scale a distribution function of con-

of the sample size or degree of disorder. A positive β-function means that the system scales towards a metal with increasing system size, while a negative β-function means that it scales towards an insulator. The metal-insulator transition is at $\beta = 0$, $\beta' > 0$. In a two-dimensional system with symplectic symmetry, such as graphene, one would expect a monotonically increasing β-function with a metal-insulator transition at [112] $\sigma_S \approx 1.4$ (see Fig. 6.1, green dashed curve).

Recent papers have argued that graphene might deviate in an interesting way from this simple expectation. Nomura and MacDonald [113] have emphasized that the very existence of a β-function in undoped graphene is not obvious, in view of the diverging Fermi wave length at the Dirac point. Assuming that one-parameter scaling does hold, Ostrovsky, Gornyi, and Mirlin [39] have proposed the scaling flow of Fig. 6.1 (black solid curve). Their β-function implies that σ approaches a universal, scale invariant value σ^* in the large-L limit, being the hypothetical quantum critical point of a certain field theory. This field theory differs from the symplectic sigma model by a topological term [39, 40]. The quantum critical point could not be derived from the weak-coupling theory of Ref. 39, but its existence was rather concluded from the analogy to the effect of a topological term in the field theory of the quantum Hall effect [111, 114]. The precise value of σ^* is therefore unknown, but it is well constrained [39]: From below by the ballistic limit[2] $\sigma_0 = 1/\pi$ [115, 116] and from above by the unstable fixed point $\sigma_S \approx 1.4$.

In this chapter we present a numerical test firstly, of the existence of one-parameter scaling, and secondly of the scaling prediction of Ref. 39 against an alternative scaling flow, a positive β without a fixed point (green dotted curve in Fig. 6.1). For such a test it is crucial to avoid the finite-a effects of intervalley scattering that might drive the system to an insulator before it can reach the predicted scale invariant regime. We accomplish this by starting from the Dirac equation, being the $a \to 0$ limit of the tight-binding model on a honeycomb lattice. We have developed an effi-

ductances [111].

[2] We call σ_0 the ballistic limit because it is reached in the absence of disorder, but we emphasize that it is a conductivity — not a conductance. This is a unique property (called "pseudodiffusive") of graphene at the Dirac point, that its conductance scales $\propto 1/L$ like in a diffusive system even in the absence of disorder.

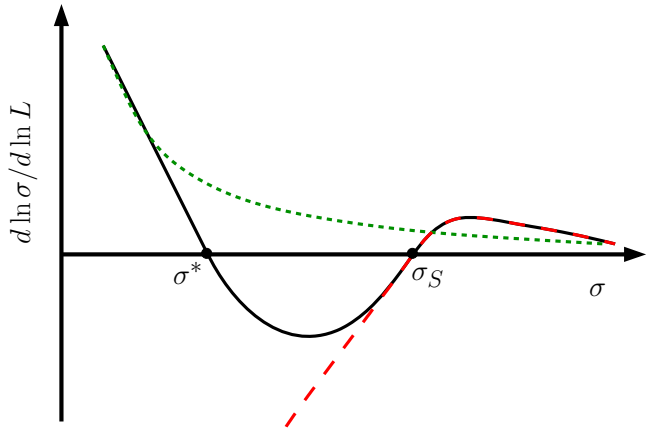

Figure 6.1. Two scenarios for the scaling of the conductivity σ with sample size L at the Dirac point in the absence of intervalley scattering. The black solid curve with two fixed points is proposed in Ref. 39, the green dotted curve without a fixed point is an alternative scaling supported by the numerical data presented in this chapter. For comparison, we include as a red dashed curve the scaling flow in the symplectic symmetry class, which has a metal-insulator transition at $\sigma_S \approx 1.4$ [112].

cient transfer operator method to solve this equation, which we describe in Sec. 6.2 before proceeding to the results in Sec. 6.3.

6.2 Transfer Matrix Approach

The single-valley Dirac Hamiltonian reads

$$H = v\mathbf{p}\cdot\boldsymbol{\sigma} + V(x) + U(x,y). \tag{6.1}$$

The vector of Pauli matrices $\boldsymbol{\sigma}$ acts on the sublattice index of the spinor Ψ, $\boldsymbol{p} = -i\hbar\partial/\partial\boldsymbol{r}$ is the momentum operator, and v is the velocity of the massless excitations. The disorder potential $U(\boldsymbol{r})$ varies randomly in the strip $0 < x < L$, $0 < y < W$ (with zero average, $\langle U\rangle = 0$). This disordered strip is connected to highly doped ballistic leads, according to the doping profile $V(x) = 0$ for $0 < x < L$, $V(x) \to -\infty$ for $x < 0$ and $x > L$. We set the Fermi energy at zero (the Dirac point), so that the disordered strip is

undoped. The disorder strength is quantified by the correlator

$$K_0 = \frac{1}{(\hbar v)^2} \int d\boldsymbol{r}' \, \langle U(\boldsymbol{r}) U(\boldsymbol{r}') \rangle. \tag{6.2}$$

Following Refs. 38 and 117, we work with a transfer operator representation of the Dirac equation $H\Psi = 0$ at zero energy. We discretize x at the N points $x_1, x_2, \ldots x_N$ and represent the impurity potential by $U(\boldsymbol{r}) = \sum_n U_n(y)\delta(x - x_n)$. Upon multiplication by $i\sigma_x$ the Dirac equation in the interval $0 < x < L$ takes the form

$$\hbar v \frac{\partial}{\partial x} \Psi_x(y) = \left[v p_y \sigma_z - i \sigma_x \sum_n U_n(y) \delta(x - x_n) \right] \Psi_x(y). \tag{6.3}$$

The transfer operator $\mathcal{M}$, defined by $\Psi_L = \mathcal{M}\Psi_0$, is given by the operator product

$$\mathcal{M} = \mathcal{P}_{L,x_N} \mathcal{K}_N \mathcal{P}_{x_N,x_{N-1}} \cdots \mathcal{K}_2 \mathcal{P}_{x_2,x_1} \mathcal{K}_1 \mathcal{P}_{x_1,0}, \tag{6.4}$$

$$\mathcal{P}_{x,x'} = \exp[(1/\hbar)(x - x') p_y \sigma_z], \tag{6.5}$$

$$\mathcal{K}_n = \exp[-(i/\hbar v) U_n \sigma_x]. \tag{6.6}$$

The operator $\mathcal{P}$ gives the decay of evanescent waves between two scattering events, described by the operators $\mathcal{K}_n$. For later use we note the current conservation relation

$$\mathcal{M}^{-1} = \sigma_x \mathcal{M}^\dagger \sigma_x. \tag{6.7}$$

We assume periodic boundary conditions in the y-direction, so that we can represent the operators in the basis

$$\psi_k^\pm = \frac{1}{\sqrt{W}} e^{i q_k y} |\pm\rangle, \quad q_k = \frac{2\pi k}{W}, \quad k = 0, \pm 1, \pm 2 \ldots. \tag{6.8}$$

The spinors $|+\rangle = 2^{-1/2} \binom{1}{1}$, $|-\rangle = 2^{-1/2} \binom{1}{-1}$ are eigenvectors of σ_x. In this basis, $(p_y)_{kk'} = \hbar q_k \delta_{kk'}$ is a diagonal operator, while $(U_n)_{kk'} = W^{-1} \int dy \, U_n(y) \times \exp[i(q_{k'} - q_k)y]$ is nondiagonal. We work with finite-dimensional transfer matrices by truncating the transverse momenta q_k at $|k| = M$.

The transmission and reflection matrices t, r are determined as in

Ref. 116, by matching the amplitudes of incoming, reflected, and transmitted modes in the heavily doped graphene leads to states in the undoped strip at $x = 0$ and $x = L$. This leads to the set of linear equations

$$\sum_k \left[\delta_{kk'}\psi_k^+(y) + r_{kk'}\psi_k^-(y)\right] = \Psi_0(y), \tag{6.9a}$$

$$\sum_k t_{kk'}\psi_k^+(y) = \Psi_L(y) = \mathcal{M}\Psi_0(y). \tag{6.9b}$$

Using the current conservation relation (6.7) we can solve Eq. (6.9) for the transmission matrix,

$$\begin{pmatrix} 1-r \\ 1+r \end{pmatrix} = \mathcal{M}^\dagger \begin{pmatrix} t \\ t \end{pmatrix} \Rightarrow t^{-1} = \langle +|\mathcal{M}^\dagger|+\rangle. \tag{6.10}$$

The transmission matrix determines the conductance $G = (4e^2/h)\,\mathrm{Tr}\,tt^\dagger$, and hence the dimensionless conductivity $\sigma = (h/4e^2)(L/W)G$. The average conductivity $\langle\sigma\rangle$ is obtained by sampling some $10^2 - 10^3$ realizations of the impurity potential.

Because the transfer matrix $\mathcal{P}$ has both exponentially small and exponentially large eigenvalues, the matrix multiplication (6.4) is numerically unstable. As in Ref. 118, we stabilize the product of transfer matrices by transforming it into a composition of unitary scattering matrices, involving only eigenvalues of unit absolute value.

We model the disorder potential $U(\boldsymbol{r}) = \sum_{n=1}^N \gamma_n \delta(x - x_n)\delta(y - y_n)$ by a collection of N isolated impurities distributed uniformly over a strip $0 < x < L$, $0 < y < W$. (An alternative model of a continuous Gaussian random potential is discussed at the end of the chapter.) The strengths γ_n of the scatterers are uniform in the interval $[-\gamma_0, \gamma_0]$. The number N sets the average separation $d = (WL/N)^{1/2}$ of the scatterers. The cut-off $|k| \leq M$ imposed on the transverse momenta q_k limits the spatial resolution $\xi \equiv W/(2M+1)$ of plane waves $\propto e^{iq_k y \pm q_k x}$ at the Dirac point. The resulting finite correlation lengths of the scattering potential in the x- and y-directions scale with ξ, but they are not determined more precisely. The disorder strength (6.2) evaluates to $K_0 = \frac{1}{3}\gamma_0^2(\hbar v d)^{-2}$, independent of the correlation lengths. We scale towards an infinite system by increasing

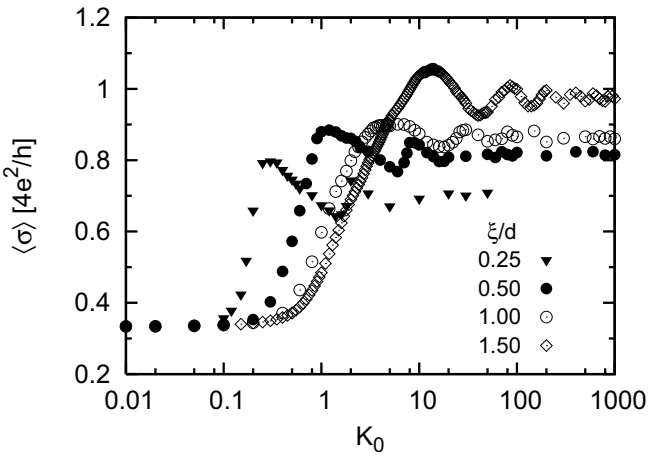

Figure 6.2. Disorder strength dependence of the average conductivity for a fixed system size ($W = 4\,L = 40\,d$) and four values of the scattering range.

$M \propto L$ at fixed disorder strength K_0, scattering range ξ/d, and aspect ratio W/L. This completes the description of our numerical method.

6.3 Numerical Results

We now turn to the results. In Fig. 6.2 we first show the dependence of the average conductivity on K_0 for a fixed system size. As in the tight-binding model of Ref. 109, disorder increases the conductivity above the ballistic value. This impurity assisted tunneling [38] saturates in an oscillatory fashion for $K_0 \gg 1$ (unitary limit [119, 120]). In the tight-binding model [109] the initial increase of σ was followed by a rapid decay of the conductivity for $K_0 \gtrsim 1$, presumably due to Anderson localization. The present model avoids localization by eliminating intervalley scattering from the outset.

The system size dependence of the average conductivity is shown in Fig. 6.3, for various combinations of disorder strength and scattering range. We take W/L sufficiently large that we have reached an aspect-ratio independent scaling flow and L/d large enough that the momentum cut-off $M > 25$. The top panel shows the data sets as a function of L/d. The in-

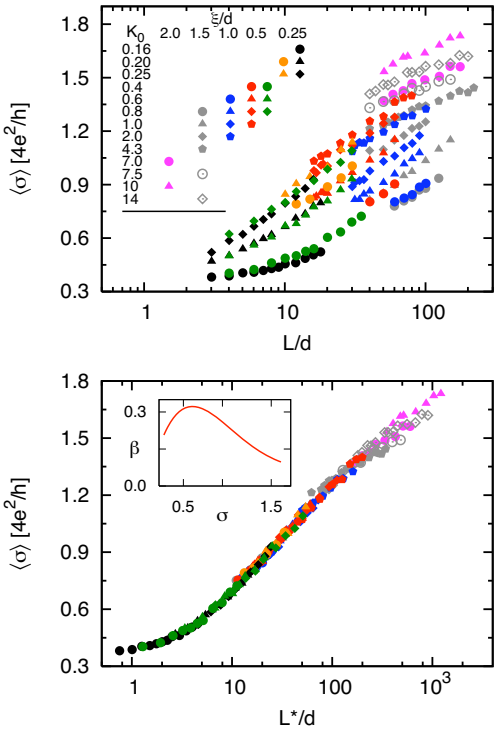

Figure 6.3. System size dependence of the average conductivity, for $W/L = 4$ (black and green solid symbols) and $W/L = 1.5$ (all other symbols) and various combinations of K_0 and ξ/d. The top panel shows the raw data. In the bottom panel the data sets have been given a horizontal offset, to demonstrate the existence of one-parameter scaling. The inset shows the resulting β-function.

crease of σ with L is approximately logarithmic, $\langle\sigma\rangle = \text{constant} + 0.25 \ln L$, much slower than the $\sqrt{L}$ increase obtained in Ref. 38 in the absence of mode mixing.

If one-parameter scaling holds, then it should be possible to rescale the length $L^* \equiv f(K_0, \xi/d)L$ such that the data sets collapse onto a single smooth curve when plotted as a function of L^*/d. (The function $f \equiv d/l^*$ determines the effective mean free path l^*, so that $L^*/d \equiv L/l^*$.) The bottom panel in Fig. 6.3 demonstrates that, indeed, this data collapse occurs. The resulting β-function is plotted in the inset. Starting from

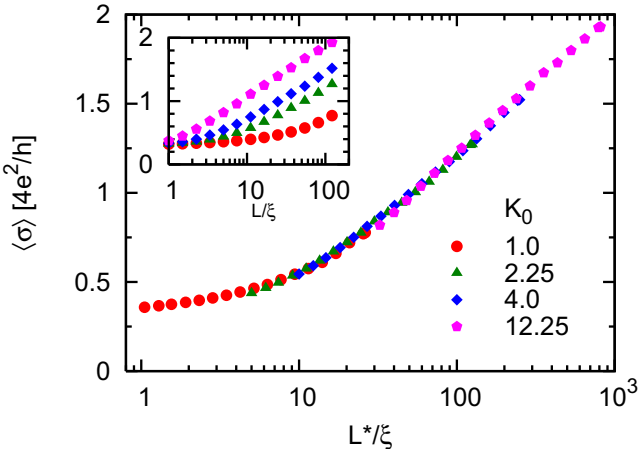

Figure 6.4. System size dependence of the average conductivity in the continuous potential model, for several values of K_0. The inset shows the raw data, while the data sets in the main plot have a horizontal offset to demonstrate one-parameter scaling when $L \gtrsim 5\,\xi$.

the ballistic limit (cf. footnote 2) at $\sigma_0 = 1/\pi$, the β-function first rises until $\sigma \approx 0.6$, and then decays to zero without becoming negative. For $\sigma > \sigma_S \approx 1.4$ the decay $\propto 1/\sigma$ is as expected for a diffusive system in the symplectic symmetry class. The positive β-function in the interval (σ_0, σ_S) precludes the flow towards a scale-invariant conductivity predicted in Ref. 39.

The model of isolated impurities considered so far is used in much of the theoretical literature, whereas experimentally a continuous random potential is more realistic [113]. We have therefore also performed numerical simulations for a random potential landscape with Gaussian correlations[3],

$$\langle U(\boldsymbol{r})U(\boldsymbol{r}')\rangle = K_0 \frac{(\hbar v)^2}{2\pi\xi^2} e^{-|\boldsymbol{r}-\boldsymbol{r}'|^2/2\xi^2}. \tag{6.11}$$

The discrete points $x_1, x_2 \ldots x_N$ in the operator product (6.4) are taken

[3]The Dirac equation with a delta-function correlated random potential has a divergent scattering rate, see, *e.g.,* Ref. 121. Hence the need to regularize the continuous potential model by means of a finite correlation length ξ.

equidistant with spacing $\delta x = L/N$, and

$$U_n(y) = \int_{x_n-\delta x/2}^{x_n+\delta x/2} dx\, U(x,y). \tag{6.12}$$

We take M, N, and W/L large enough that the resulting conductivity no longer depends on these parameters. We then scale towards larger system sizes by increasing L/ξ and W/ξ at fixed K_0. No saturation of σ with increasing K_0 is observed for the continuous random potential (as expected, since the unitary limit is specific for isolated scatterers [119, 120]). Fig. 6.4 shows the size dependence of the conductivity — both the raw data as a function of L (inset) as well as the rescaled data as a function of $L^* \equiv g(K_0)L$. Single-parameter scaling applies for $L \gtrsim 5\,\xi$, where $\langle\sigma\rangle = \text{constant} + 0.32 \ln L$. The prefactor of the logarithm is about 25% larger than in the model of isolated impurities (Fig. 6.3), which is within the numerical uncertainty.

6.4 Conclusion

In conclusion, we have demonstrated that the central hypothesis of the scaling theory of quantum transport, the existence of one-parameter scaling, holds in graphene. The scaling flow which we find (green dotted curve in Fig. 6.1) is qualitatively different both from what would be expected for conventional electronic systems (red dashed curve) and also from what has been predicted [120] for graphene (black solid curve). Our scaling flow has no fixed point, meaning that the conductivity of undoped graphene keeps increasing with increasing disorder in the absence of intervalley scattering. The fundamental question "what is the limiting conductivity σ_∞ of an infinitely large undoped carbon monolayer" has therefore three different answers: $\sigma_\infty = 1/\pi$ in the absence of any disorder [115, 116], $\sigma_\infty = \infty$ with disorder that does not mix the valleys (this chapter), and $\sigma_\infty = 0$ with intervalley scattering [36, 37].

After the work described in this chapter was finished similar conclusions have been reported by Nomura, Koshino, and Ryu [122].